EMISSIVITIES OF γ AND $e^{\pm}$ INDUCED BY COLLISIONS BETWEEN COSMIC-RAY PROTON AND ISM IN THE GALAXY

T. Shibata[1], Y. Ohira[1], K. Kohri[2], and R. Yamazaki[1]

[1] *Department of Physics and Mathematics, Aoyama-Gakuin University, Kanagawa 229-8558, Japan*
[2] *KEK Theory Center and the Graduate University for Advanced Studies (Sokendai), 1-1 Oho, Tsukuba 305-0801, Japan*

ABSTRACT

We show that the production cross-sections of γ and $e^{\pm}$ in p-p collision, $\sigma_{pp\to\gamma}$ and $\sigma_{pp\to e^{\pm}}$ respectively, may be kinematically equivalent without back to that of the parent pion $\sigma_{pp\to\pi}$. So we can obtain straightforwardly $\sigma_{pp\to e^{\pm}}$ once we have $\sigma_{pp\to\gamma}$ with help of the machine data. We discuss in detail the relation between them, and present how reliable for $\sigma_{pp\to e^{\pm}}$ even in the TeV region. Based on these studies, we give also the emissivities of γ and $e^{\pm}$ in the Galaxy, and present the positron fraction observed at the solar system, the ratio of e^+ to $[e^+ + e^-]$. It is now in a vital open question that it appears to rise as the energy gets higher, $\gtrsim 10\,\mathrm{GeV}$, far beyond the expectation with the standard model today. The aim of the present paper is to give the production cross-section of $e^{\pm}$ firmly even in the TeV region, in order to see quantitatively how much deviated from the standard model in the yield of $e^{\pm}$ and its propagation to the Earth.

Subject headings: cosmic rays — Galaxy: structure — gamma-rays: positrons, cross section

1. Introduction

Nowadays the *direct* observations of antimatters such as the antiproton ($\bar{\mathrm{p}}$) and positron (e^+) are available with the on board experiments even in the higher energy region $\gtrsim 100\,\mathrm{GeV}$, particularly by PAMELA (Adriani et al. 2009a, 2009b) and AMS-02, while the full result of the latter is not yet reported in this stage.

Since the early reports of the anomaly in the antiproton flux around 1980 (Golden et et al. 1979; Bogomolov et al. 1979; Buffington et al. 1981), they have always brought us something new beyond the standard model in both particle-physics and the astrophysics, while difficult to induce the origin of the anomaly mainly due to the limited observations in removing the atmopsheric $\bar{\mathrm{p}}$'s, modulation effects, in statistics, and so on. Unfortunately we do not catch a signal of the anomaly in the $\bar{\mathrm{p}}$ spectrum today even with the sophisticated modern instruments developed by, for instance BESS (Haino et al. 2004) and PAMELA (Adriani et al. 2009a) at least up to 100 GeV, which is explained by the standard model in the source and the subsequent propagation to the Earth within the uncertainties in the choice of numerical parameters in modeling.

Alternatively HEAT (DuVernois et al. 2001) reported a possibility of the anomaly in the positron flux in 1995 in connection with the WIMPs (Weakly Interacting Massive Particles), indicating an excess of e^+ in the higher energy region as compared to the expectation with the standard model, and many obsevations for the antimatter search have been performed continuously up to now with these early studies.

Recently PAMELA (Adriani et al. 2009a) gives the positron fraction, the ratio of positrons (e^+'s) to electrons (e^-'s) plus e^+'s, covering the very wide energy ranges with $0.1 \sim 150\,\mathrm{GeV}$ with high statistics. FERMI (Ackermann et al. 2011) also gives the positron fraction in 20-150 GeV consis-

tent with the PAMELA, while not direct observation, but the *semi-direct* one removing the background protons in the all positive charged particles with the simulation calculations. All these results indicate that the positron fraction rises above 10 GeV up to 100 GeV.

Under these situations, the AMS-02 is ready to make clear the possibility of positron excess with higher statistics and unprecedented precision, expected to cover the very wide energy ranges, 0.1 $\sim$ 300 GeV.

With the dvelopments of these observations on the antiparticles, the theoretical explanations for the anomaly in the positron exess have been also extensively studied from the various points of view, dark matter scenario (Hisano et al. 2009a, 2009b; Ishiwata et al. 2009; see http://pamela.roma2.infn.it/ for a complete list of references), pulsars (Büsching et al. 2008; Hopper et al. 2009; Kawanaka et al. 2010), supernova explosions happened in the dense gas cloud (Fujita et al. 2009), reacceleration of secondaries in the source environments (Blasi 2009; Mertsch and Sarkar 2009; Stawarz et al. 2010), and other models (e.g., Ioka 2010; Kashiyama et al. 2011; Kisaka and Kawanaka 2012).

It has been pointed out, however, that there exist many uncertainties in both observations and theories for the anomaly, for instance in statistics, the energy resolution, the particle identification for the former, and artificial assumptions in the elementary processes for the latter, such as the cross-section of the dark matter annihilation, the mechanism for the escape of the pairs from the pulsar, and so forth. However, the uncertainties in the former would be much reduced soon by the AMS-02 as mentioned above, so that the theoretical interpretations and the parameter sets in the assumption must be much more improved without worring about the experimental uncertainties.

The aim of the present paper is not to give the explanations for the anomaly indicated by several groups today, but to provide definitely the cross-sections for the production of γ and $e^{\pm}$ in p-p collision and the emissivity of these elements in the Galaxy based on the machine data, covering the very wide energy ranges in the projectile proton even with LHCf (Adriani et al. 2011), 1 GeV $\sim$ 20 PeV in the laboratory frame (hereafter L.F.). Through these studies, we expect definitely how much excess appears in the experimental data on the positron fraction as compared to the standard model for the production and the subsequent propagation of the cosmic-ray (CR) elements in the Galaxy. The theoretical speculations will be reported elsewhere in the near future with the coming results of AMS-02.

One must worry much about the reliability of the production cross-section for γ and $e^{\pm}$ in p-p collision for the machine data, among which we should remark particularly the *energy* distribution, $d\sigma/dE_\pi$, in pion production, which is much more important than the angular (pseudo-rapidity) distribution, $d\sigma/d\eta_\pi$ with η_π=-$\ln\tan\frac{\theta}{2}$, as practically we observe the energy spectra of photons in the wide energy ranges.

However, from the experimental point of view in the machine data, it is generally very difficult to measure the energy distribution of secondary pions, particularly in the high energy region within the forward cone in the center of mass frame (hereafter C.M.F.) because of the concentration of secondaries in such limited cone, while rather easy for the pseudo-rapidity distribution in the central region.

As compared to the charged pions, it is easier for the energy estimation of γ's via π^0 even in the high energy and forward regions, by setting the calorimeter with far distance from the vertx point, separable enough in the jammed γ's, for instance see the LHCf experiments (Sako et al. 2007; Mase et al. 2012) for the detail. This is the reason why we have focussed so much upon the data on γ itself in place of the parent charged pions. In fact, LHCf group (Adriani et al. 2012) gives us recently unprecedented data on γ's with TeV energy in C.M.F., see Figure 14 in Appendix B, and Paper I (Sato et al. 2012) for the detail.

We have already presented the production-cross section of γ's empirically in p-p collision covering the energy region $E_0 = 1\,\mathrm{GeV} \sim 20\,\mathrm{PeV}$ in Paper I, and have confirmed that it reproduces nicely various kinds of obaservables, pseudo-rapidity, Feymann variable in addtion to the energy spectrum of γ. In the present work, we apply it for the production cross-section of $e^{\pm}$, and point out that the production of γ and $e^{\pm}$ via pion is kinematically equivalent, resulting in that we may not need back to the parent pion once we construct the production cross-section for γ.

It would be worth mentioning in advance that we separate the secondary mesons into two components phenomenologically, the pionization and the isobar ones, the former corresponding to the central collision with the average transverse momentum of $\bar{p}_t \approx 300\,\mathrm{MeV}$, and the latter to the peripheral one with small momentum transfer, and/or with the Pomeron exchange.

In the present paper, we do not take into account the hard process with the large momentum transfer mainly effective around the central region in the C.M.F. as its cross-section is much smaller than that of the soft one with $\bar{p}_t \approx 300\,\mathrm{MeV}$, and we are interested only in reproducing the cross-section of γ-ray production, particularly in the forward region.

The contribution of the isobar component is determined so that well reproduced are the experimental data on the energy dependence of the multiplicity of mesons (see Section 4.1). In Section 7, we present the positron fraction based on our semi-empirical production cross-section for γ and $e^{\pm}$, combining it with the standard propagation model from the emission site, $\boldsymbol{r}$, to the solar system (SS), $\boldsymbol{r}_{\odot}$. The theoretical implications of the result will be discussed elsewhere in the near future with the coming AMS-02 data.

2. Production cross-section of secondary products in pionizaion components

Before going to the main subject to obtain various kinds of cross-section, we touch briefly the familiar rapidity-variable η corresponding to a particle velocity $v\,(= c\beta)$ since it appears very often in the present work, well simplifying the procedure in derivation of the cross-section we are interested in,

$$\eta = \frac{1}{2}\ln\frac{1+\beta}{1-\beta} = \ln(\gamma + \sqrt{\gamma^2 - 1}), \qquad (1)$$

with

$$\gamma = \frac{1}{\sqrt{1-\beta^2}}; \quad \beta = \frac{v}{c}. \qquad (2)$$

For the practical numerical calculations, we had better use the second relation in Equation (1), since the first expression often gives rise to divergence for $\beta \to 1$ in the very high energy region, while the first one is much more common in current textbooks than the second. So we define a following rapidity-function $\eta(\gamma)$, regarding it as a function of the Lorentz factor γ

$$\eta(\gamma) = \ln(\gamma + \sqrt{\gamma^2 - 1}), \qquad (3)$$

which appears often in the present work.

With use of the rapidity η_s of a secondary particle s with mass m_s, we have well-known expresions for the energy and momentum with $c = 1$,

$$E_s = m_s \cosh\eta_s; \quad P_s = m_s \sinh\eta_s, \qquad (4)$$

with

$$d\eta_s = dE_s/P_s. \qquad (5)$$

In the following discussion, we call β simply as a particle velocity in units of c.

2.1. Decay products coming from pions

Let us introduce two energy distribution functions, $\Phi(E_0, E_\pi)$ and $\varphi(E_0, \epsilon_s)$, each for a parent pion π ($\equiv \pi^0$, $\pi^{\pm}$) with energy E_π (P_π in momentum) in the L.F. and for its decay product s ($\equiv$ "γ", "$\mu^{\pm}$") with *kinetic* energy ϵ_s ($= E_s - m_s$) respectively, and E_0 is *kinetic* energy of a projectile proton in the L.F.,

$$\varphi(E_0, \epsilon_s) = \int_{E_\pi^-}^{E_\pi^+} \frac{\Phi(E_0, E_\pi)}{1-\kappa_s^2}\frac{dE_\pi}{P_\pi}, \qquad (6)$$

with

$$\frac{E_\pi^{\pm}}{E_s} = \frac{(1+\kappa_s^2) \pm (1-\kappa_s^2)\beta_s}{2\kappa_s^2}, \qquad (7)$$

where β_s is the velocity of s and $\kappa_s = m_s/m_\pi$. Namely, two types of decay, $s \equiv \gamma,\ \mu$, are *equivalent* in the decay kinematics but with the mass difference only. Note that Equation (7) holds even in the case of $\kappa_s = 0$ with $[m_s, \beta_s] \to [0, 1]$ in π^0-2γ decay. See Equation (13) for the explcit form of $E_\pi^{\pm}$ in such a decay mode. So $\varphi(E_0, \epsilon_s)$ is the common function often appearing in the present paper.

2.2. Energy spectrum of γ-rays via π^0-2γ decay

In Paper I (Sato et al. 2011), we present explicitly the energy spectrum of γ-rays in the L.F., $\varphi(E_0, E_\gamma)$, based on the *raw* machine data *without* referring to π^0, pointing out that we do not

need to worry about the contributions from other neutral mesons such as $\eta, \eta', \ldots$

Using $\varphi(E_0, E_\gamma)$ given by Equation (6), we have a semi-emiprical energy spectrum of γ-rays

$$\frac{dN_\gamma}{dE_\gamma} = \bar{N}_\gamma \varphi(E_0, E_\gamma), \tag{8}$$

explcit form of which is given in Paper I, after the integration over the emission angle θ,

$$\frac{\varphi(E_0, E_\gamma)}{\beta_{\rm C}^2 \Theta_{\rm C}} = \frac{1}{M_{\rm p}} \int_{\omega_-}^{\omega_+} \frac{(1 - x\Gamma_\theta)^4}{\Gamma_\theta + \zeta\tau_\theta} {\rm e}^{-\tau_\theta x} d\omega, \tag{9}$$

with

$$\omega_\pm = \beta_c^{-1} - \beta_c^{\pm 1} {\rm e}^{\pm \eta_0^* - \eta_\gamma^*}. \tag{10}$$

Here, $x = E_\gamma/E_0$, $\omega = \cos\theta$, and

$$\eta_0^* = \ln(2\beta_c\gamma_c M_{\rm p}/m_{\pi^0}), \tag{11}$$

$$\eta_\gamma^* = \ln(2\beta_c\gamma_c E_\gamma/m_{\pi^0}), \tag{12}$$

and β_c (γ_c) is the velocity (Lorentz factor) of C.M.F. with respect to the L.F., $M_{\rm p}$ the mass of proton, see Appendix A for $[\tau_\theta, \Gamma_\theta]$ and $[\Theta_c, \zeta]$. Note $P_{\rm p}^* = \beta_c\gamma_c M_{\rm p}$ in Equation (11) is the momentum of projectile (and/or target) proton in the C.M.F.. In Equation (10), we have to keep in mind $\omega_- = -1$ for $E_\gamma < \frac{1}{2} m_{\pi^0} {\rm e}^{-(\eta_0^* + \eta_c)}$ (η_c: rapidity of the C.M.F. with $\eta_c \equiv \eta(\gamma_c)$ in Equation (3)).

Now, while we have used an approximation $E_\pi^- = E_\gamma$ in Paper I as we have interested in the energy region $E_\gamma \gtrsim m_{\pi^0}$, we use the exact relation given by Equation (7) in the present paper,

$$E_\pi^- \equiv \epsilon_\gamma = E_\gamma + \frac{m_{\pi^0}^2}{4E_\gamma}; \quad E_\pi^+ = E_0, \tag{13}$$

namely we replace E_γ with ϵ_γ except E_γ in $\omega_\pm$ given by Equation (10) as it comes froms the kinematical constraint in emission angle.

Another expression of E_π^- ($\equiv \epsilon_\gamma$) is

$$E_\pi^- = m_{\pi^0} \cosh\eta_\gamma, \tag{14}$$

$$\eta_\gamma = \ln(2E_\gamma/m_{\pi^0}), \tag{15}$$

which is useful for the upper and lower limits of pion energy in the electron production as discussed in the next section, remembering that a rapidity variable η in L.F. shifts by $\eta - \eta_c$ in C.M.F., where η_c is the rapidity of the latter frame against the former one.

Corresponding to the above replacement, $E_\gamma \to \epsilon_\gamma$, we replace $x = (E_\gamma/E_0)$ in the integrand of Equation (9) by

$$x_\gamma = \frac{\epsilon_\gamma}{E_0} = x + \frac{m_{\pi^0}^2}{4xE_0^2}, \tag{16}$$

so that $x_\gamma \approx x$ for $E_0 \gg m_{\pi^0}$, justifying that the results presented in Paper I are applicable enough over wide energy region we are interested in but in the low energy region $E_0 \lesssim M_{\rm p}$.

Here we have to take care of the normalization constant Θ_c which was normalized so that the integration over $x = [0, 1]$ for Equation (9) leads to the average γ-ray multiplicity $\bar{N}_\gamma$ in Equation (8) (see also Equation (10) in Paper I). Instead, we *renormalize* Θ_c so that

$$\int_{E_\gamma^-}^{E_\gamma^+} \varphi(E_0, E_\gamma) dE_\gamma = 1, \tag{17}$$

with

$$E_\gamma^\pm = \frac{1}{2} m_{\pi^0} {\rm e}^{\pm(\bar{\eta}_\pi^* + \eta_c)}, \tag{18}$$

where $\bar{\eta}_\pi^*$ is the maximum rapidity of π^0 in the C.M.F. given by

$$\bar{\eta}_\pi^* = \eta(\bar{\gamma}_\pi^*); \quad \bar{\gamma}_\pi^* = \beta_c \cosh\eta_0^*, \tag{19}$$

see Equations (3) and (11) for $\eta(\bar{\gamma}_\pi^*)$ and η_0^* respectively, and $\bar{\eta}_\pi^* \approx \eta_0^*$ for $E_0 \gg M_{\rm p}$ ($\beta_c \approx 1$).

See Appendix A for the detail of the relation between the previous normalization constant Θ_c and the present one after the replacement of x by x_γ.

2.3. Energy spectrum of e$^\pm$ via $\pi^\pm$- $\mu^\pm$- e$^\pm$ decay

The electron and/or positron with energy $\check{E}_e$ are created by the three-body decay from a fully polarized muon, $\mu^\pm \to {\rm e}^\pm + \nu_e(\bar{\nu}_e) + \bar{\nu}_\mu(\nu_\mu)$, the production of which is kinematically equivalent to γ (see Equation (6)) through the isotropic two-body decay as discussed in the last Section 2.2.

Now, the energy-angular distribution of electron (positron) in the muon rest frame is given by

$$g(\check{q}, \check{\theta}) = \check{q}^2(3 - 2\check{q}) \left[1 + \xi \cos\check{\theta} \frac{1 - 2\check{q}}{3 - 2\check{q}}\right], \tag{20}$$

(Commins 1973; Orth and Buffington 1976), where $\check{q} = 2\check{E}_e/m_\mu$, and $\xi = +1$ (-1) for electron (positron), and $\check{\theta}$ is the angle between the electron and the spin of muon in the muon rest frame.

In practice we need the energy distribution of $e^\pm$, $f(E_\pi, E_e)$, for a parent pion with *fixed* energy E_π in the L.F. after the integration over the energy and the emission angle of intermediate muon, taking the polarization effect into account. The full expression of $f(E_\pi, E_e)$ is summarized by Dermer (1986), while somewhat tedious to evaluate.

In the present paper, we resummarize it with use of a rapidity variable η_π, introducing a function ϕ,

$$f(E_\pi, E_e)dE_e = \phi(\eta_\pi, q_e)\frac{dE_e}{P_\pi}, \tag{21}$$

and in Table 1 we present it explicitly with use of three parameters, $[q_e; \eta_\pi, \tilde{\eta}_\mu]$, which are given by

$$q_e = 2E_e/m_\mu, \tag{22}$$

$$E_\pi = m_\pi \cosh \eta_\pi, \tag{23}$$

with $\eta_\pi \equiv \eta(\gamma_\pi)$, and $\tilde{\eta}_\mu \equiv \eta(\tilde{\gamma}_\mu)$ in Equation (3).

Namely, q_e is the electron (positron) energy E_e in units of half of the muon mass in the L.F., and two rapidity variables, η_π and $\tilde{\eta}_\mu$, correspond to that of the parent pion in the L.F. and to that of the daughter muon in the pion rest frame respectively, with $\tilde{\gamma}_\mu = \frac{1}{2}(m_\mu/m_\pi + m_\pi/m_\mu) = 1.039$, leading to $\tilde{\eta}_\mu = 0.2783$ with $\tilde{\beta}_\mu = 0.2714$. See also Table 2 for $[g_1(Q),\ g_2(Q)]$ with $Q \equiv q_e e^{\pm\eta_\pi}$, $e^{\pm\tilde{\eta}_\mu}$ in $\phi(\eta_\pi, q_e)$, and Table 3 for three parameters $[G_0;\ g_{1,0},\ g_{2,0}]$ appearing in $[g_1, g_2]$ together with their explcit numerical values for the electron $(\xi = +1)$ and positron $(\xi = -1)$.

In Figure 1(a), we present the numerical value of $\phi(\eta_\pi, q_e)$ against $q_e \exp[-(\eta_\pi + \bar{\eta}_\mu)]$ for three pion *kinetic* energies, $\epsilon_\pi \equiv E_\pi - m_\pi = 0.01$, 0.1, and 1 GeV in the case of electron (green curves) and positron (red curves). One finds that $\phi(\eta_\pi, q_e) \approx \phi(q_e e^{-\eta_\pi})$ for $\epsilon_\pi \gtrsim 1\mathrm{GeV}$, namely $\phi(\eta_\pi, q_e)$ scales in the form of $\phi(E_e/E_\pi)$ in the high energy region, as naturally expected.

One should remark that the normalization in Equation (21) holds exactly, taking care of the restriction with $q_e \subseteq [q_e^-, q_e^+]$ in Table 1

$$\int_{E_e^-}^{E_e^+} \phi(\eta_\pi, q_e)\frac{dE_e}{P_\pi} = 1, \tag{24}$$

with

$$E_e^- = 0; \quad E_e^+ = \frac{1}{2}m_\mu e^{\eta_\pi + \tilde{\eta}_\mu}. \tag{25}$$

Once we have the normalized energy spectrum of $e^\pm$ coming from the $\pi^\pm$-$\mu^\pm$ decay in the L.F., we obtain straightforwardly the production energy spectrum of $e^\pm$ in p-p collision (see Equation (6) for Φ)

$$\frac{dN_{e^\pm}}{dE_e} = \bar{N}_{\pi^\pm}\int_{E_\pi^-}^{E_\pi^+} \Phi(E_0, E_\pi)f(E_\pi, E_e)dE_\pi, \tag{26}$$

with

$$E_\pi^\pm = m_\pi \cosh \eta_\pi^\pm, \tag{27}$$

where $\bar{N}_{\pi^\pm}$ $(\equiv \bar{N}_{\pi^\pm}(E_0))$ is the effective multiplicity of charged pions, depending on the projectile proton energy E_0, and

$$\eta_\pi^- = \bar{\eta}_e - \tilde{\eta}_\mu; \quad \eta_\pi^+ = \bar{\eta}_\pi^* + \eta_c, \tag{28}$$

with $\bar{\eta}_e = \ln q_e$, and $\bar{\eta}_\pi^*$ is the maximum rapidity of pion in the C.M.F. given by Equation (19), namely η_π^+ is the maximum one in the L.F..

Another expression of E_π^- in Equation (27) is given by

$$E_\pi^- = E_e + \frac{m_\pi^2}{4E_e}, \tag{29}$$

which is the same form as Equation (13) for γ-ray energy spectrum.

Now remarking the relation in Equation (7) with $[E_\pi^-, E_\pi^+] = [\epsilon_\gamma, E_0]$ in the case of π^0-2γ decay, we have

$$\left.\frac{\partial \varphi}{\partial \epsilon}\right|_{\epsilon = E_\pi - m_\pi} = -\Phi(E_0, E_\pi)\frac{1}{P_\pi}, \tag{30}$$

and using Equation (21), eventually we obtain

$$\frac{dN_{e^\pm}}{dE_e} = \bar{N}_{\pi^\pm}\int_{\eta_\pi^-}^{\eta_\pi^+} \varphi(E_0, \epsilon_\pi)\phi^\dagger(\eta_\pi, q_e)d\eta_\pi, \tag{31}$$

where we use a relation $dE_\pi/P_\pi = d\eta_\pi$, see Equations (19) and (28) for $\eta_\pi^\pm$, and ϵ_π $(\equiv E_\pi - m_\pi)$ is the kinetic energy of pion in the L.F expressed with use of η_π as

$$\epsilon_\pi = 2m_\pi \sinh^2 \frac{\eta_\pi}{2}. \tag{32}$$

In Figure 1(b), we present the numerical values of $\phi^\dagger(\eta_\pi, q_e)$ against $q_e \exp[-(\eta_\pi + \bar{\eta}_\mu)]$ for three

kinetic energies of the parent pion corresponding to Figure 1(a), and again we find the scaling nature in $\phi^\dagger(E_e/E_\pi)$ similarly as in $\phi(E_e/E_\pi)$ in the high energy region $\epsilon_\pi \gtrsim 1\,\mathrm{GeV}$.

Note that the energy spectra of two products, γ and $\mathrm{e}^\pm$, are both expressed with use of the common cross-section $\varphi(E_0,\epsilon)$ given by Equation (9) with $\epsilon \equiv \epsilon_\gamma, \epsilon_\pi$, namely the two production cross-sections, Equations (8) and (31), are kinematically equivalent in the sense that they are linked by a *model-independent* function $\phi(\eta_\pi, q_e)$, without referring back to $\Phi(E_0,E_\pi)$, the very model-dependent cross-section.

3. Production cross-section of secondary products in isobaric components

In the low energy region around $E_0 \approx 1{-}3\,\mathrm{GeV}$, many isobaric components such as $\mathit{\Delta}(1232)$, $\mathit{\Delta}(1410)$, ... as well as the exclusive channel $pp \to \pi^+ d$ (d: deuteron) become effective for secondaries in addition to those coming from the pionization component mentioned in the last section.

In this section we consider their contributions in an approximate way so that reproduced are the experimental data on the production cross-section of secondaries, particularly for π^0 and π^+, while not effective for other mesons, π^-, $\mathrm{K}^\pm$, and so on (see Figure 3).

3.1. Energy spectrum of γ-rays via Δ - π^0- 2γ decay

We assume that an isobar with mass M_Δ is produced in p-p collision, disintegrating isotropically into π^0 $(+\ p)$ or π^+ $(+\ n)$ with the pion energy $\tilde{E}_\pi$ in the *isobar* rest frame, and thus we have immediately

$$\tilde{E}_\pi = m_\pi \tau_\Delta \cosh\tilde{\eta}_\Delta, \qquad (33)$$

$$\tilde{\eta}_\Delta = \ln(\tau_\Delta M_\Delta/m_\pi), \qquad (34)$$

with

$$\tau_\Delta = \sqrt{1 - M_\mathrm{p}^2/M_\Delta^2}, \qquad (35)$$

note that M_Δ must be set with the condition of $\tilde{E}_\pi \geq m_\pi$. One may remark that $\tau_\Delta \cosh\tilde{\eta}_\Delta$ in Equation (33) is the Lorentz factor $\tilde{\gamma}_\pi$ of the pion in the isobar frame as presented in Equation (39).

So, the energy distribution of pions in the L.F. is of the uniform one, straightforwardly written as

$$\Phi_\Delta(E_0,E_\pi)dE_\pi = \Phi_0(E_0)dE_\pi, \qquad (36)$$

where Φ_0 is determined from the following normaliztion procedure.

The pion energy in the L.F. produced through the isobar disintegration is bound to the range, $\tilde{E}_\pi^- \leq E_\pi \leq \tilde{E}_\pi^+$, with

$$\tilde{E}_\pi^\pm = m_\pi \cosh(\eta_\Delta^* + \eta_c \pm \tilde{\eta}_\pi), \qquad (37)$$

leading to

$$\Phi_0(E_0) = \frac{1/(2\tilde{P}_\pi)}{\sinh(\eta_\Delta^* + \eta_c)}. \qquad (38)$$

Here $\tilde{\eta}_\pi$ ($\tilde{P}_\pi = m_\pi\tilde{\beta}_\pi\tilde{\gamma}_\pi$) is the rapidity (momentum) of pion in the isobar rest frame, and η_Δ^* the rapidity of the isobar in the C.M.F., each given by

$$\tilde{\eta}_\pi = \eta(\tilde{\gamma}_\pi); \quad \tilde{\gamma}_\pi = \tau_\Delta \cosh\tilde{\eta}_\Delta, \qquad (39)$$

$$\eta_\Delta^* = \eta(\gamma_\Delta^*); \quad \gamma_\Delta^* = \tau_\Delta \cosh\eta_s^*, \qquad (40)$$

with

$$\eta_s^* = \ln(\sqrt{s}/\tau_\Delta M_\Delta), \qquad (41)$$

see Equation (34) for $\tilde{\eta}_\Delta$, and $\sqrt{s} = 2M_\mathrm{p}\gamma_c$ (center of mass energy). Note that $\eta_\Delta^* + \eta_c$ in Equation (37) is the rapidity of isobar, η_Δ, in the L.F..

Now, similarly as Equation (6), we obtain immediately the energy distribution of γ-rays coming from the isobaric components with $[E_\pi^-, E_\pi^+] = [\epsilon_\gamma, E_0]$,

$$\varphi_\Delta(E_0,\epsilon_\gamma) = \int_{\epsilon_\gamma}^{E_0} \Phi_\Delta(E_0,E_\pi)\frac{dE_\pi}{P_\pi}, \qquad (42)$$

leading to

$$\frac{dN_\gamma^\Delta}{dE_\gamma} = \bar{N}_\gamma^\Delta \Phi_0(E_0)[\eta_\mathrm{p} - \eta_\gamma], \qquad (43)$$

where $\bar{N}_\gamma^\Delta$ is the effective multiplicity of γ-rays (via π^0) through the Δ-isobar disintegration, and η_p is the rapidity of projectile proton in the L.F., and η_γ the minimum rapidity of pion given by Equation (15) to produce γ with the energy of E_γ.

3.2. Energy spectrum of e^+ via Δ - π^+- μ^+- e^+ decay

As the contribution of e^- from the isobaric component is negligibly small in comparison with e^+ around a few GeV, we consider here the energy spectrum of e^+ only.

Similarly to Equation (26), we obtain immediately the positron production cross-section coming from the isobar decay, $\Delta \to \pi^+ \to \mu^+ \to e^+$,

$$\frac{dN^{\Delta}_{e^+}}{dE_e} = \bar{N}^{\Delta}_{\pi^+} \int_{E_\pi^-}^{E_\pi^+} \Phi_\Delta(E_0, E_\pi) f(E_\pi, E_e) dE_\pi, \tag{44}$$

where $\bar{N}^{\Delta}_{\pi^+}$ is the effective multiplicity of π^+ through the disintegration of Δ-isobar, and see Equation (27) for $E_\pi^{\pm}$.

With use of $\Phi_0(E_0)$ (see Equation (38)) in $\Phi_\Delta(E_0, E_\pi)$, we obtain immediately

$$\frac{dN^{\Delta}_{e^+}}{dE_e} = \bar{N}^{\Delta}_{\pi^+} \Phi_0(E_0) \int_{\eta_\pi^-}^{\eta_\pi^+} \phi(\eta_\pi, q_e) d\eta_\pi, \tag{45}$$

see Equations (19) and (28) for $\eta_\pi^{\pm}$.

Here we have to take care of the integration with respect to η_π in the above equation, which must be perfomed separately with the range of η_π. It depends on the positron energy E_e $(= 2m_\mu q_e)$, see the restriction $q_e \subseteq [q_e^-, q_e^+]$ in Table 1.

Now, one must note that the energy spectra of the secondary products, γ and e^+, coming from both the pionization and the isobaric components given by Equations (8), (31), (43) and (45), are all expressed with use of ϕ, $\phi^\dagger$, and $\int \phi \, d\eta_\pi$ alone, apart from the basic function $\varphi(E_0, \epsilon)$, where the second distribution function $\phi^\dagger$ corresponds to the differential of the first one with respect to η_π, and the third function to the integral of the first one.

See next section for the explicit numerical value of the parameters appearing above, M_Δ, $\bar{N}^{\Delta}_{\gamma}$, and so on.

4. Multiplicity of secondary particles

In the last section, we present the production cross-sections for γ and $e^{\pm}$ in p-p collisions, $[dN_\gamma/dE_\gamma,\ dN_{e^\pm}/dE_e]$ from the pionization components, and $[dN^{\Delta}_{\gamma}/dE_\gamma,\ dN^{\Delta}_{e^+}/dE_e]$ from the isobaric ones respectively, where the *average* multiplicity of secondaries, $[\bar{N}_\gamma,\ \bar{N}_{\pi^\pm}]$ and $[\bar{N}^{\Delta}_{\gamma},\ \bar{N}^{\Delta}_{\pi^+}]$, appearing in each cross-section respectively, depend on the energy of projectile proton E_0. These numerical values should be determinded from the machine data.

4.1. Parametrization in the empirical formulae

In this paper, we slightly modify the formula, $\bar{N}_\gamma(E_0)$, on the average multiplicity presented in Paper I in order to apply it also for charged components, $\pi^{\pm}$ and $K^{\pm}$, while the contributions of charged kaons are not important practically as discussed later.

As mentioned in Paper I, we should regard $\bar{N}_s(E_0)$ as an *effective* multiplicity, particularly in the high energy region, say $E_0 \gtrsim$ TeV, since the low energy secondaries are not effective in the galactic phenomena.

We summarize it below

$$\bar{N}_s(E_0) = \bar{N}_0 \varLambda_s(\hat{E}_0) \hat{E}_0^{0.115}, \tag{46}$$

with

$$\hat{E}_0 = E_0 - E_{\rm th}, \tag{47}$$

and

$$\varLambda_s(\epsilon) = \left[1 - e^{-\sqrt{\epsilon/\varepsilon_1}}\right]\left[1 - e^{-\sqrt[4]{\epsilon/\varepsilon_2}}\right] e^{-(\epsilon_c/\epsilon)^k}, \tag{48}$$

where numerical values of $\bar{N}_0, E_{\rm th}, \epsilon_c, \ldots$, are presented in Table 4 for individual secondaries, $s \equiv \gamma,\ \pi^+, \ldots$, while $[\epsilon_1, \epsilon_2] = [4.53\text{GeV},\ 1.98\text{TeV}]$ irrespective of s.

For the multiplicity of γ and π^+ through the disintegration of Δ-isobar, we assume

$$\bar{N}^{\Delta}_s(E_0) = \bar{N}^{\Delta}_0 \exp\left[-\left(\frac{\ln \hat{E}_0/M_\Delta}{\ln m_\pi}\right)^2\right], \tag{49}$$

where $\bar{N}^{\Delta}_0 = [0.61,\ 0.15]$ for $s \equiv [\pi^+, \gamma]$ respectively, and $E_{\rm th} = 0.290\text{GeV}$ $(\approx 2m_\pi)$, the same as the threshold energy of π^+ production (see Table 4).

We assume $M_\Delta = 1.25$ GeV, leading to $[\tilde{E}_\pi, \tilde{\eta}_\pi]$ $= [0.279\text{GeV}, 2.0]$ from Equations (33) and (39) respectively, which is determined so that reproduced are the experimental data on the multiplicities of γ and π^+ as presented in Figures 2 and 3, particularly for π^+ in the low energy region (green dotted curves).

4.2. Comparison with the experimental data on the multiplicity

Let us compare experimental data with the present parameterizations on the production cross-sections and the (effective) multiplicity of both γ-rays and charged mesons (Stecker 1973; Dermer 1986; Antinucci et al. 1973; Sato et al. 2012). See Paper I for the more complete comparison between them in addition to the multiplicity, where presented were various kinds of physical quantities such as pseudo-rapidity, Feynman variable, γ-ray energy ... in both the C.M.F. and L.F., covering very wide energies up to the LHC, $E_0 = 1\,\mathrm{GeV} \sim 20\,\mathrm{PeV}$.

In Figure 2, we present simultaneously the production cross-section of γ-rays, $\sigma_{\mathrm{pp}}\bar{N}_\gamma$, (righthand-side axis) and its average multiplicity, $\bar{N}_\gamma$, (lefthand-side axis) against E_0, where σ_{pp} is the total inelastic collision cross-section (see Paper I). One may note that those coming from the isobaric components are not significant in the case of $\pi^0 \to 2\gamma$.

In this figure, we plot additionally two points (open and filled red squares symbols) at $E_0 \approx 400\,\mathrm{TeV}$ based on the most recent LHCf data with $\sqrt{s} = 900\mathrm{GeV}$ (Adriani et al. 2012) which is obtained by fitting our empirical curve in C.M.F.. See Equation (18) and Figure 14 in Paper I, and also Figure 14 in Appendix B of the present paper for the fitting result.

In Figure 3, we show the production cross-section and the average multiplicity for charged mesons (Stecker 1973; Dermer 1986; Antinucci et al. 1973; Sato et al. 2012), corresponding to Figure 2 for γ-rays, where we present also the empirical curves given by Equations (46) and (49) with use of the numerical values in Table 4 in both Figures 2 and 3.

Here we present the contributions of π^+ separately coming from both the pionization and isobaric components, and one finds that the latter is effective only around a few GeV with $\bar{N}_0^\Delta = 0.61$ (green dotted curves around a few GeV), while not effective for $\pi^0 \to 2\gamma$ from M_Δ-disintegration with $\bar{N}_0^\Delta = 0.15$ in Figure 2, so that we do not present it explicitly as in Figure 3, but only the superposed ones (solid curves).

From Figure 3, one finds that the contribution of $\mathrm{K}^\pm$ are on average of as large as 7% in all charged mesons for $E_0 \gtrsim 10\,\mathrm{GeV}$ and negligible below, so that the contribution to $\mathrm{e}^\pm$ coming from $\mathrm{K}^\pm$ would be of the same magnitude. Thus, in the practical numerical calculations, we consider only $\pi^\pm$ as the source of secondary $\mathrm{e}^\pm$'s, but take 7% increase for them due to kaon effect into acount finally.

5. Comparison with other numerical codes for the elementary processes

Nowadays many elaborative codes for the elementary processes in the galactic phenomena have been extensively developed, and become increasingly important as the new observational data such as FERMI and AMS-02 have become available with pretty high quality in both the statistics and precision. In this section we compare our calculations on the production cross-sections of γ, $\mathrm{e}^\pm$ in p-p collision with those expected from three calculations by (a) Dermer (1986; analytical method), (b) Kamae et al. (2006; simulational one), and (c) PYTHIA-code (Sjostrand et al. 2006).

5.1. Production cross-section for γ

In Figures 4(a-c), we present the production cross-section on γ's in p-p collision, each with (a) Dermer, (b) Kamae, and (c) PYTHIA, for $E_0 = 10^0, 10^1, 10^2, 10^3, 10^4\,\mathrm{GeV}$, while Dermer presents only for the first three, and PYTHIA gives only for those except the first energy (not applicable in the low energy region $\lesssim 10\,\mathrm{GeV}$). In these figures we plot their results in the form of several discrete points alone in order to avoid the complexty for the comparison.

We find that they are more or less compatible with each other, while one may claim that there exists some deviation with each other. The small deviation would be not important in study of, for instance, the diffused components, γ and/or $\mathrm{e}^\pm$, in the low energy region $\lesssim 100\,\mathrm{GeV}$, and it must be masked by the observational uncertainties in practice, even if exists.

However, it might become serious in the higher energy region, say more that 1 TeV. In fact one may worry about small (but systematic) deviation in the energy spectrum in the higher energy region, $E_0 = 1,\ 10\,\mathrm{TeV}$, and it maybe amplified more in much higer energy.

This might be due to the fact that the machine data they have based are rather in the low energy, $\lesssim$TeV, while the present one covers even TeV-γ's based on the recent LHCf data, see Figure 14 in Appendix B as an example, and Paper I for the detail in TeV and higher. TeV-γ astronomy will be available in the near future, particularly after the full observation by CTA-program starts around 2020 (CTA Consortium 2012).

5.2. Production cross-section for $e^{\pm}$

In Figures 5(a-c) and 6(a-c) we present the production cross-sections on positrons and electrons respectively corresponding to γ's as presented in Figures 4(a-c). Our results seem to be similar to those by Dermer in the low energy region but electrons at $E_0 = 1$ GeV in Figure 6(a), and we find again there exists some dicrepancy between ours and others in the high energy region.

Unfortunately we may have no user-friendly experimental data for $E_0 \gtrsim 5 \times 10^5$ GeV on the production of secondary electrons (positrons) via π-μ decay, but as emphasized in Section 2 the cross-sections for productions of γ and $e^{\pm}$ are equivalent in kinematics, model-independently linked with each other. So we should ask the reliability of the production cross-section of $e^{\pm}$ for that of γ which is available enough in current machine data. In such a sense, those for $e^{\pm}$ must be also reliable enough over the wide energy ranges, as we have confirmed that our parameterization in the production-cross section of γ's is applicable well even in the LHC energy region.

5.3. Spectral-weighted moment in γ-ray yield

In practice, important is the following spectral-weighted moment for a given projectile energy E_0 $(= E_\gamma/x)$

$$Z_\gamma(E_0) = \int_0^1 x^{\beta-1}\sigma_{pp\to\gamma}(E_0, xE_0)E_0 dx, \quad (50)$$

where β is the index of the differential proton energy spectrum with $E_0^{-\beta}$, and note $d/dE_\gamma = E_0 d/dx$. $Z_\gamma(E_0)$ must be independent of E_0 if the Feynman scaling holds exactly. On the otherhand, it has been well-known for a long time that such a scaling nature is surely broken through the study of various cosmic-ray components (electromagnetic and hadronic components) in the atmosphere (for instance, Konishi et al. 1976).

Let us present the above moment against the projectile energy E_0 in the case of $\beta = 2.6$ - 3.0 (index of the proton spectrum in the Galaxy), corresponding to γ $(= \beta - 1/3) = 2.26$ - 2.66 (index of the source proton spectrum), in Figure 7, where plotted together are other several results (QGSJET-II, SIBYLL, and Kamae) summarized by Kachelrieß and Ostapchencko (2012). All results indicate that the scaling nature breaks slowly, particularly in the higher energy region $\gtrsim 1$ TeV, but not drastically, which is consistent with the past studies for the atmopsheric CR diffusions in both electromagnetic and hadronic components.

6. Emissivities of secondary γ and $e^{\pm}$ in the Galaxy

Once we obtain the production cross-section in p-p collision, $\sigma_{pp\to s}(E_0, E_s)$ $(s \equiv \gamma, e^{\pm})$, we can estimate easily the emissivities of γ and $e^{\pm}$ in the Galaxy coming from the interaction between CR-proton and the ISM,

$$q_{pp\to s}(E_s, \boldsymbol{r}) = \quad (51)$$

$$\int_{E_{\min}}^{\infty} N_{\rm p}(E_0, \boldsymbol{r})[n(\boldsymbol{r}) v \sigma_{pp\to s}(E_0, E_s)]dE_0, \quad (52)$$

with

$$\frac{\sigma_{pp\to s}(E_0, E_s)}{\sigma_{pp}(E_0)} = \frac{dN_s}{dE_s}(E_0, E_s), \quad (53)$$

where $n(\boldsymbol{r})$ is the gas density at $\boldsymbol{r}$, and σ_{pp} is the inelastic total collision cross-section (see Paper I).

The minimum projectile energy $E_{\min}$ is given by the familiar form

$$E_{\min}^{(s)} = E_s + \frac{m_\pi^2}{4E_s}; \quad (s \equiv \gamma, e^{\pm}), \quad (54)$$

which is presented in Equations (13) and (29), giving the same form irrespective of s. But in the practical calculation, we have to take account of the threshold energy effect in the pion production, namely $E_{\min} = \mathrm{Max}[E_{\rm th}, E_{\min}^{(s)}]$ with $E_{\rm th} \approx 2m_\pi$. In this section we present the emissivities of γ and $e^{\pm}$ at several observation points $\boldsymbol{r}$ in the Galaxy.

6.1. Normalization of the proton and the primary-electron fluxes

As given by Equation (52), we need two critical inputs, the absolute proton density, $N_{\rm p}(E_0, \boldsymbol{r})$, and the ISM gas density, $n(\boldsymbol{r})$, in addtion to the production cross-section, $\sigma_{pp\to s}$, to estimate the emissivity of the secondary product s at $\boldsymbol{r}$, $q_{pp\to s}(E_s, \boldsymbol{r})$.

For the former input, we use here the observational data on the absolute proton flux at a normalization energy $\bar{E}_n = 100\,$GeV, which is free from the modulation effect as well as from the observational uncertainty in both statisics and the experimental precision, while scatters considerably in the higher energy region $\gtrsim 1\,$TeV. It would be, however, improved greatly very soon after the full results by AMS-02.

Let us present the explcit value of the proton density, $\bar{N}^{\odot}_{n,{\rm p}} \equiv N_{\rm p}(\boldsymbol{r}_\odot, \bar{E}_n)$, at $(E_0, \boldsymbol{r}) = (\bar{E}_n, \boldsymbol{r}_\odot)$,

$$c\bar{N}^{\odot}_{n,{\rm p}} = 6.16 \times 10^{-1}\ ({\rm m^{-2}s^{-1}GeV^{-1}}), \tag{55}$$

based on the current proton flux at $E_0 = 100\,$GeV,

$$E_0^{2.5}\frac{dI^{\odot}_{\rm p}}{dE_0} = 4.90 \times 10^{3}\ ({\rm m^{-2}s^{-1}sr^{-1}GeV^{1.5}}), \tag{56}$$

which is consistent with the past (Derbina et al. 2005) and the most recent PAMELA data (Adriani et al. 2011).

In addition to the absolute proton density, we need also the absolute electron density at the normalization energy $\bar{E}_n = 100\,$GeV in the following

$$c\bar{N}^{\odot}_{n,{\rm e}} = 1.82 \times 10^{-3}\ ({\rm m^{-2}s^{-1}GeV^{-1}}), \tag{57}$$

based on the current electron flux at $E_{\rm e} = 100\,$GeV mainly focussing on FERMI (Ackermann et al. 2010), PAMELA (see Figure 9), and the ECC data most recently revised by Kobayashi et al. (2012),

$$E_{\rm e}^{3}\frac{dI^{\odot}_{\rm e}}{dE_{\rm e}} = 1.45 \times 10^{2}\ ({\rm m^{-2}s^{-1}sr^{-1}GeV^{2}}), \tag{58}$$

which is important to see the positron fraction to all electrons, ${\rm e}^+/({\rm e}^+ + {\rm e}^-)$ as seen later.

Here we have to separate $c\bar{N}^{\odot}_{n,{\rm e}}$ into two components, one from (1) the primary electrons, and the other from (2) the secondary electrons induced by the charged pions via $\pi^\pm$- $\mu^\pm$- ${\rm e}^\pm$ decays,

$$c\bar{N}^{\odot}_{n,{\rm e}} = c\bar{N}^{\odot}_{n,1} + c\bar{N}^{\odot,\pm}_{n,2}, \tag{59}$$

while the contribution of the second components is of as large as 10% around 100 GeV.

With the above normalizations for the proton and electron spectra, and if we assume the indices of source spectra for two elements are common with γ, and given by

$$Q_{\rm p}(E_{\rm p}) = Q_{0,{\rm p}}E_{\rm p}^{-\gamma}, \tag{60}$$

$$Q_{\rm e}(E_{\rm e}) = Q_{0,{\rm e}}E_{\rm e}^{-\gamma}, \tag{61}$$

we can obtain the absolute emissivities of them at the *source*, $Q_{0,{\rm p}}$ and $Q_{0,{\rm e}}$, with help of the solution of the transport equations, while depending on the source index γ (see Paper II). We summarize them in Table 5 for $\gamma = 2.27$, 2.37, and 2.47, corresponding to the indices at the SS with β ($=\gamma + \alpha$) $= 2.6$, 2.7, and 2.8 with $\alpha = 1/3$ respectively.

6.2. Emissivities of various kinds of observables

For the ISM gas density in Equation (52), we use an empirical one for $n(\boldsymbol{r})$ presented in Paper II (Shibata et al. 2011), which is based on the GALPROP-code (http://www.gamma.mpe.-garching.mpg.de./~aws/aws.html), nowadays the most standard one extensively developed by Strong and Moskalenko (1998).

In Figure 8 we present the emissivity of γ and ${\rm e}^\pm$ all together at two sites, (r, z) = (a) $(\boldsymbol{r}_\odot, 0)$ and (b) $(\boldsymbol{r}_\odot, 1{\rm kpc})$ with $\boldsymbol{r}_\odot = 8.5\,$kpc, each corresponding to that at the SS and at 1kpc in vertical direction above the galactic plane respectively, where we show γ's due to two electromagnetic processes together, the bremsstrahlung (EB-γ; sky-blue curves) and the inverse compton (IC-γ; blue curves) induced by the interaction between *primary* electrons and the ISRF(see Paper II).

From these results, we find the emissitivites of the secondary products coming from the proton, γ (green curves), ${\rm e}^+$ (red curves), and ${\rm e}^-$ (purple curves), are all dominant for $E_i \gtrsim 1$ GeV ("i" $\equiv \gamma$, ${\rm e}^\pm$) at the SS in comparison with γ's coming from the primary electrons due to the EB (blue-sky curves) and the IC (blue curves).

The energies at the maximum emissivities of secondary products, γ's and ${\rm e}^\pm$'s, are around $m_{\pi^0}/2 \approx$ 60-70 MeV for γ, and $m_{\mu^\pm}/3 \approx$ 30-50 MeV for ${\rm e}^\pm$ respectively, as naturally expected from the two-body decay in $\pi^0 \to 2\gamma$, and the three-body decay in $\mu^\pm \to e^\pm\nu\bar{\nu}$.

7. Positron fraction in all electrons, $e^- + e^+$

Now we give the positron fraction in all electrons ($e^+ + e^-$), which is obtained by combining the emissivity $q_{pp\to e^\pm}(E_e, \boldsymbol{r})$ at $\boldsymbol{r}$ presented in the last section with the solution of the transport equation $P(\boldsymbol{r}_\odot, E_e^\odot; \boldsymbol{r}, E_e)$, where we need the absolute intensities for both protons and the electrons as mentioned in the last section. See Paper II (Shibata et al. 2011) for the procedure to combine $q_{pp\to e^\pm}(E_e, \boldsymbol{r})$ with $P(\boldsymbol{r}_\odot, E_e^\odot; \boldsymbol{r}, E_e)$.

First in Figure 9, we show the energy spectrum for all electrons together with the present calculations for three spectrum indices, $\beta = 2.6$, 2.7, and 2.8, all normalized at 100 GeV, where we present curves with four modulation parametrs, $\Phi = 200$, 400, 600, and 800 MV, using the force field approximation (Gleeson and Axford 1968). See Derbina et al. (2005) for the energy spectrum for hadronic components, proton, helium, and so on.

In Figure 10, we present the current experimental data on the positron fraction to all electrons, $e^+/(e^+ + e^-)$, together with our calculations for three spectral indices, $\beta = 2.6$, 2.7, and 2.8, where again assumed are four modulation parameters as in Figure 9.

One may claim that PAMELA data and our curves deviate significantly from AMS-01, HEAT, etc. at low energies $\lesssim 5$ GeV. The deviation is understood in the framework of the charge-sign-dependent solar modularion, and its effect is well studied with the drift model (Moskalenko et al. 2002). According to Beischer et al. (2009), they find the PAMELA data is consistent enough with the pre-PAMELA ones such as AMS-01 (Alcaraz et al. 2000; Aguilar et al. 2007), HEAT (Beatty et al. 2004), CAPRICE (Boezio et al. 2000), and TS93 (Golden et al. 1996), using the GALPLOP code with the charge-sign-modulation, while including great uncertinties in the modeling as yet.

Fortunaley they show explicitly the correlation between the positron fraction $e^+/(e^+ + e^-)$ and the positron energy E_e every data points with and without the charge-sign-modulation based on the GALPROP code. Thus taking the charge-sign-dependent modulation into account, we give our corrected curves in Figure 11, together with the corrected data, where four data, AMS-01, HEAT, ACAPRICE, and TS93, are all combined with some statistical weights. Now we find good agreement each other in the low energy region, while we should keep in mind that the correction is not model-independent one, including much uncertainties in modulation modeling such as heliospheric magnetic field, the tilt of the current sheet, and so forth.

Of course, important is the positron fraction in the high energy $\gtrsim 5$ GeV as often pointed out by past works (for example Moskalenko and Strong 1998; Delahaye et al. 2010), and clearly the enhancement in the fraction appears, while the present result seems to be more significant than those expected from GALPROP one in the high energy. Uncertainties in both data and calculations related to the modulation will be reduced by AMS-02.

8. Discussion and summary

With use of the refined production cross-section for $e^\pm$ given by Equations (8), (31), (43) and (45), we give its emissivity $q_{pp\to e^\pm}(E_e, \boldsymbol{r})$ at $\boldsymbol{r}$ in the Galaxy, and the positron fraction, $e^+/(e^+ + e^-)$, at the SS combining $q_{pp\to e^\pm}$ with the propagation function, $P(\boldsymbol{r}_\odot, E_e^\odot; \boldsymbol{r}, E_e)$. As reported by the previous works, we find again the significant discrepany between the numerical calculations based on the standard model and the observational results.

Now, we must touch upon the contributions from the heavy components, He, . . ., Fe as we have focused only on the proton. Unfortunately nowadays we have not yet enough data on the nuclei effects in the multiple meson productions, while various theoretical models are proposed, reproducing in thier own way the machine data.

About this critical uncertainty we have introduced the so called "enhancement factor", defined by

$$\varepsilon_s(\boldsymbol{r}, E_s) = q_{\text{all}\to s}(\boldsymbol{r}, E_s)/q_{pp\to s}(\boldsymbol{r}, E_s), \qquad (62)$$

with $s \equiv \gamma$, $e^\pm$, $\bar{p}, \ldots$, where $q_{\text{all}\to s}$ is the *total emissivity* of secondary s including all CR elements (projectiles) as well as the helium gas (targets) in the ISM, while $q_{pp\to s}$ from only p-p interactions. As presented in Shibata et al. (2000, 2007), the magnitude of ε_s is approximately around 1.5-1.6, depending very weakly on $(s; \boldsymbol{r}, E_s)$. Several authors (Stephens & Badhwar 1981; Gaisser & Schafer 1992; Cavallo & Gould

1971; Dermer 1986) also give the enhancement factor with nearly the same magnitude, but using slightly different definition without the energy dependence. This tells us that the choice of the model in the nucleus-nucleus interaction does not give rise to any serious effect. In practice we assume $\varepsilon_s = 1.53$ irrespective of $s \equiv \gamma, \mathrm{e}^{\pm}$.

In order to estimate the positron fraction, we normalize both proton and primary electron fluxes at 100 GeV, reliable enough even today as the statistics is rather rich with small scatterings around there as seen from Figure 9. However, we should not forget that the spectral shape, i.e., the spectral index β in both components is quite essential in both lower and the higher energy regions, particularly in the latter, while the change of the index in the former may be masked by the solar modulation.

In fact, if we assume another spectral shape (or energy-dependent one) in the primary components either with softer or harder ones, one must get another conclusion on the positron fraction. For instance, recent data on the proton and the helium spectra by ATIC (Wefel et al. 2008), CREAM (Ahn et al. 2010) and PAMELA (Adriani et al. 2011) report all the drastic hard spectrum in the high energy region $\gtrsim$ 100-200 GeV, which must result in the hard spectrum of positrons in the higher energy region.

In contrast to these critical indications, we assume here rather conservative ones with $\beta = 2.6$ - 2.8 independent of the primary energy and the species. These uncertainties in the observations must be removed very soon by the coming AMS-02 data as repeatedly reffered, which will bring us not only the $\mathrm{e}^{\pm}$ spectra, but also the unprecedented spectra for hadronic componets, proton, helium, ..., as well as the B/C, $^{10}\mathrm{Be}/^{9}\mathrm{Be}$, etc..

In the near future, we will study the origin of the anomaly in positron fraction from the theoritical point of view, based on the present results as well as the unprecedented data by AMS-02, where the uncertainties in both observation and the modeling must be much reduced.

Acknowledgments

Two of authors (T. S. and R. Y) deeply appreciate Research Institute, Aoyama-Gakuin University for helping and progressing our research by the fund. This work is supported in part by Grant-in-Aid for Scientific research from the Ministry of Education, Science, Sports, and Culture (MEXT), Japan, No. 21111006, No. 22244030, No. 23540327 (K. K.), and No. 24.8344 (Y. O.).

APPENDIX A

Summary of the variables defined in Paper I and the numerical value of the renormalization constant.

In this appendix, we summarize several variables introduced in Paper I, and present the numerical values of the renormalized constant Θ_c, comparing with the previous one.

First we give below parameters in the L.F. appearing in Equation (9),

$$\tau_\theta = 2(\gamma_{\mathrm{C}}^2 - 1)(M_{\mathrm{p}}/p_0)\sin\theta, \tag{63}$$

$$\Gamma_\theta = 2(\gamma_{\mathrm{C}}^2 - 1)(1 - \beta_{\mathrm{C}}\cos\theta). \tag{64}$$

In Paper I, putting $x^* = E_\gamma^*/T_c = 2E_\gamma^*/\sqrt{s}$ ($\sqrt{s}$: center of mass energy) with $\tau_c = T_c/p_0$, we assume $0 \le x^* \le 1$, leading to a following normalization constant Θ_0 (defined as Θ_c in Paper I) so that we have an average γ-ray multiplicity after the integration over the all phase space in the distribution function,

$$\frac{1}{\Theta_0} = \int_0^1 \frac{F_0(\tau_\theta^*)}{1+\zeta\tau_\theta^*} d(\cos\theta^*);\quad \tau_{\theta^*} = \tau_c \sin\theta^*, \tag{65}$$

with $\zeta = 0.02$, and

$$F_\ell(\tau) = \int_0^1 (x^*)^\ell (1-x^*)^4 \mathrm{e}^{-\tau x^*} dx^*, \quad (\ell = 0, 1). \tag{66}$$

p_0 in τ_θ corresponds to the average transverse momentum of γ-rays, $\bar{p}_t$, given by

$$\frac{\bar{p}_{\mathrm{t}}}{p_0} = \int_0^1 \frac{\tau_\theta^* F_1(\tau_\theta^*)}{1+\zeta\tau_\theta^*} d(\cos\theta^*) \Bigg/ \int_0^1 \frac{F_0(\tau_\theta^*)}{1+\zeta\tau_\theta^*} d(\cos\theta^*). \tag{67}$$

and the average transverse momentum $\bar{p}_t$ is determined from the experimental data, depending (very weakly) on E_0 (=$\hat{E}_0 + E_{\mathrm{th}}$), given by

$$\bar{p}_{\mathrm{t}}(E_0) = m_\pi \hat{E}_0^{\,0.0286} \left[1 - \exp\left(-1.156\sqrt[4]{\hat{E}_0}\right)\right]. \tag{68}$$

As presented in Equation (9) in the text, we do not use an approximation with $x = E_\gamma/E_0$, but the exact one with $x_\gamma = x + m_{\pi^0}^2/4xE_0^2$ in the L.F. as given by Equation (16). Corresponding to the replacement of x by x_γ, Θ_0 is replaced by

$$\frac{1}{\Theta_c} = \frac{\beta_c^2 E_0}{M_\mathrm{p}} \int_{x_-}^{x_+} dx \int_{\omega_-}^{\omega_+} \frac{(1 - x_\gamma \Gamma_\theta)^4}{\Gamma_\theta + \zeta\tau_\theta} \mathrm{e}^{-\tau_\theta x_\gamma} d\omega, \tag{69}$$

with

$$x_\pm = (m_{\pi^0}/E_0)\mathrm{e}^{\pm(\eta_\pi^* + \eta_c)}, \tag{70}$$

where $\omega_\pm$ is given by Equation (10) and see (19) for η_π^* in $x_\pm$.

In Figure 12, we present the previous normaliztion Θ_0 (dotted curve) and the renormalized one Θ_c (broken dotted one), where we present the ratio Θ_c/Θ_0 against E_0 (solid curve) together to see the effect of the replacement of x by x_γ. One finds some difference between them in the energy region $E_0 \lesssim 10\,\mathrm{GeV}$, while not effective in the higher energy region with the constant ratio ($\sim 20\%$ higher than the previous one in absolute value).

APPENDIX B
Fitting of the production cross-section with the machine data.

We have already compared our empirical cross-section in detail in Paper I with the machine data in the wide energy ranges, $E_0 = 1\,\mathrm{GeV} \sim 20\,\mathrm{PeV}$, and find the present parameterization reproduces nicely the data even for the energy spectrum by LHC. However, as presented in Section 2.2, we use the exact minimum energy E_π^- in π^0 decay given by Equation (13), not E_γ but ϵ_γ, which deforms slightly the cross-section in the low energy region $E_0 \lesssim 1\,\mathrm{GeV}$, while negligible in the higher energy region.

So in Figure 13, we give again the γ-ray energy spectrum with the revised normalization as presented in Appendix A in the case of $E_0 = 0.97\,\mathrm{GeV}$, where we present both empirical ones, the previous one (dotted curve) and the present one (solid one). Thus we find the previous one does not reproduce the data for $E_\gamma \gtrsim 0.7\,\mathrm{GeV}$ as naturally expected, while the present one reproduces well the drop due to the constraint in the phase space.

After Paper I, a new data of LHCf with $\sqrt{s} = 900\,\mathrm{GeV}$ is reported (Adriani et al. 2012), so that we additionally show the fitting result in Figure 14, reconfirming the present parameterization reproduces again excellently the production cross-section in the extremely high energy region, in contrast to the fitting in the very low energy region in Figure 13.

In Figure 14 two production cross-sections are demonstrated with two emission angles, one with $\bar{\theta} = 39\,\mu\mathrm{rad}$ (solid square) and the other with $\bar{\theta} = 234\,\mu\mathrm{rad}$ (open square). One must note that our parametrization reproduces surprisingly well the data with the set $[\bar{N}_\gamma, p_0]$ = [30.2-35.2, 188MeV/c], which are plotted onto Figure 2 in the text.

Anyway our parameterization reporduces the experimental data from GeV to PeV with a simple form given by Equation (6).

REFERENCES

Ackermann, M. et al. 2010, Phys. Rev. D, 82, 092004

Ackermann, M. et al. 2011, arXiv:1109.0521v1 [astro-ph.HE] 2 Sep 2011

Adriani, O., et al. 2009a, Nature 458, 607 (2009)

Adriani, O., et al. 2009b, Phys. Rev. Lett., 105, 121101 (2009)

Adriani, O., et al. 2011, Phys. Lett. B, 703, 128

Adriani, O., et al. 2012, arXiv:1207.7183v1 [hep-ex] 31 Jul 2012

Alcaraz, J., et al. (AMS Collaboration) 2007, Phys. Lett. B 646, 145

Alcaraz, J., et al. (AMS Collaboration) 2000, Phys. Lett. B 484, 10

Antinucci, M., et al., CERN-Bologna ISR Collaboration, 1973, Nuovo Cimento Lett. 6, , 121

Ahn, H.S. et al. 2010, ApJ, 714, L89

Beatty, J.J. et al. (HEAT Collaboration) 2004, Phys. Rev. Lett. 93, 241102

Beischer, B., Doethinchem, P., Gast, H., Kirn, T., and Schael, S. 2009, New J. Phys. 11, 105021

Boezio, M. et al. (ACAPRICE Corraboration) 2000, ApJ, 532, 653

Bogomolov, F.A. et al. 1979, Proc. 16th Int. Cosmic Ray Conf., (Kyoto), 1, 330

Buffington, A. et al. 1981, ApJ, 248, 1179

Blasi, P. 2009, Phys. Rev. Lett., 103, 051104 (2009)

Büsching, I., deJager, O.C., Potgieter, M.S., and Venter, V., 2008, ApJ, 678, L39

Cavallo, G., and Gould, R.J. 1971, Nuovo Cimento, 2B, 77

Commins, E. 2005, 1973, *Weak Interactions* (New York: McGraw-Hill)

The CTA Consortium 2010, arXiv:1008.3703v3 [astro-ph.IM] 11 Apr 2012

Derbina, V. A., et al. 2005, ApJ, 628, L41

Dermer 1986, ApJ, 307, 47

DuVernois, M.A., et al. 2001, ApJ, 559, 296

Fujita, Y., Kohri, K., Yamazaki, R., and Ioka, K. 2009, Phys. Rev., D80, 063003

Gaisser, T.K., and Schaefer, R.K. 1992, ApJ, 394, 174

Gleeson, I.J., and Axjord, W.I. 1968, ApJ, 154, 1011

Golden, R. L., et al. 1979, Phys. Rev. Lett. 43, 1196

Golden, R. L., et al. (TS93 Collaboration) 1996, ApJ, 457, L103

Haino, S., et al. Phys. Lett. B, 545, 1135

Hisano, J., Kawasaki, M., Kohri, K., and Nakayama, K. 2009a, Phys. Rev., D79, 063514

Hisano, J., Kawasaki, M., Kohri, K., and Nakayama, K. 2009b, Phys. Rev., D79, 083522

Hopper, D., Blasi, P., and Serpico, P.D., J. Cosmol. Astrop. Phys. 1, 025 (2009) Phys. Rev., D79, 083522

Ioka, K. 2010, Prog. Theor. Phys. 123, 743

Ishiwata, K., Matsumoto, S., and Moroi, T. 2009, Phys. Lett. B675, 446

Kachelrieß M. and Ostapchenko, S. 2012, arXiv:1206.4705v1 [astro-ph.HE] 24 Jul 2012

Kamae, T., et al. 2006, ApJ, 647, 692

Kashiyama, K., Ioka, K., and Kawanaka, N. 2011, Phys. Rev. D, 83, 023002

Kawanaka, N., Ioka, K., and Nojiri, M. M. 2010, ApJ, 710, 958

Kisaka, S. and Kawanaka, N. 2012, MNRAS, 421, 3543

Kobayashi, T., et al. 2012, ApJ, 760, 146

Mase, T. et al., 2012, Nucl. Instrum. Methods A, 671, 129

Mertsch, P. and Sarkar, S. 2009, PRL 103, 081104

Orth, C.D. and Buffington, A. 1976, ApJ, 206, 312

Sako, T. et al., 2007, Nucl. Instrum. Methods A, 578, 146

Sato, H., Shibata, T., and Yamazaki, R. 2012, Astropart. Phys. 36, 83 (Paper I)

Shibata, T., Honda, N., and Watanabe, J., 2007, Astropart. Phys., 27, 411

Shibata, T., Futo, Y., and Sekiguchi, S. 2008, ApJ, 678, 907

Shibata, T., Ishikawa, T., and Sekiguchi, S. 2011, ApJ, 727, 38 (Paper II)

Sjostrand, T., Mrenna, S., and Skands, P. 2006, J. High Energy Phys., 05, 026

Stawarz, L., Petrosian, V., and Blandford, R. 2010, ApJ, 710, 236

Stecker, F.W. 1973, Astropart. Phys. J. 185, 499

Stephens, S.A., and Badhwar, G.D. 1981, Ap & SS, 76, 213 Astropart. Phys. J. 185, 499

Strong, A. W., and Moskalenko, I. V. 1998, ApJ, 509, 212

Suzuki, R., Watanabe, J., and Shibata, T. 2005, Astropart. Phys., 23, 510

Wefel, J. et al. 2008, Proc. 31th Int. Cosmic Ray Conf., (Lodz), 2, 31

Table 1

Summary of the normalized distribution function of $e^{\pm}$-spectrum, $\phi(\eta_\pi, q_e)$ and its derivative $\phi^\dagger(\eta_\pi, q_e)$, resulting from a charged pion decay, $\pi^\pm \to \mu^\pm \to e^\pm$, where the muon is created fully polarized, left-handed for π^+ decay and right-handed for π^- decay. In this table, we use a parameter, $q_e = 2E_e/m_\mu$, and two rapidities, $\tilde{\eta}_\mu$ $(= 0.278)$ and η_π, each correspondint to that of muon in the pion rest frame and that of pion in the L.F., respectively. See Table 2 for $[g_1(Q),\ g_2(Q)]$ and $[g_1^\dagger(Q),\ g_2^\dagger(Q)]$ with $Q \equiv q_e \mathrm{e}^{\pm\eta_\pi},\ \mathrm{e}^{\pm\tilde{\eta}_\mu}$.

$\phi(\eta_\pi, q_e)$	$\phi^\dagger(\eta_\pi, q_e)$	$q_e \subseteq [q_e^-,\ q_e^+]$	$\eta_\pi \lesseqgtr \tilde{\eta}_\mu$
$g_1(q_e\mathrm{e}^{\eta_\pi}) - g_1(q_e\mathrm{e}^{-\eta_\pi})$	$g_1^\dagger(q_e\mathrm{e}^{\eta_\pi}) + g_1^\dagger(q_e\mathrm{e}^{-\eta_\pi})$	$[0,\ \mathrm{e}^{-(\eta_\pi+\tilde{\eta}_\mu)}]$	——
$g_2(q_e\mathrm{e}^{\eta_\pi}) - g_2(\mathrm{e}^{-\tilde{\eta}_\mu}) + g_1(\mathrm{e}^{-\tilde{\eta}_\mu}) - g_1(q_e\mathrm{e}^{-\eta_\pi})$	$g_2^\dagger(q_e\mathrm{e}^{\eta_\pi}) + g_1^\dagger(q_e\mathrm{e}^{-\eta_\pi})$	$[\mathrm{e}^{-(\eta_\pi+\tilde{\eta}_\mu)},\ \mathrm{e}^{-\lvert\eta_\pi-\tilde{\eta}_\mu\rvert}]$	——
$g_2(q_e\mathrm{e}^{\eta_\pi}) - g_2(q_e\mathrm{e}^{-\eta_\pi})$	$g_2^\dagger(q_e\mathrm{e}^{\eta_\pi}) + g_2^\dagger(q_e\mathrm{e}^{-\eta_\pi})$	$[\mathrm{e}^{-\lvert\eta_\pi-\tilde{\eta}_\mu\rvert},\ \mathrm{e}^{+\lvert\eta_\pi-\tilde{\eta}_\mu\rvert}]$	$\eta_\pi < \tilde{\eta}_\mu$
$g_2(\mathrm{e}^{\tilde{\eta}_\mu}) - g_2(\mathrm{e}^{-\tilde{\eta}_\mu}) + g_1(\mathrm{e}^{-\tilde{\eta}_\mu}) - g_1(q_e\mathrm{e}^{-\eta_\pi})$	$g_1^\dagger(q_e\mathrm{e}^{-\eta_\pi})$	$[\mathrm{e}^{-\lvert\eta_\pi-\tilde{\eta}_\mu\rvert},\ \mathrm{e}^{+\lvert\eta_\pi-\tilde{\eta}_\mu\rvert}]$	$\eta_\pi > \tilde{\eta}_\mu$
$g_2(\mathrm{e}^{\tilde{\eta}_\mu}) - g_2(q_e\mathrm{e}^{-\eta_\pi})$	$g_2^\dagger(q_e\mathrm{e}^{-\eta_\pi})$	$[\mathrm{e}^{+\lvert\eta_\pi-\tilde{\eta}_\mu\rvert},\ \mathrm{e}^{+(\eta_\pi+\tilde{\eta}_\mu)}]$	——
0	0	$[\mathrm{e}^{+(\eta_\pi+\tilde{\eta}_\mu)},\ \infty]$	——

Table 2

Summary of $[g_1(Q),\ g_1^\dagger(Q)]$ and $[g_2(Q),\ g_2^\dagger(Q)]$ appearing in Table 1 with $Q \equiv q_e\mathrm{e}^{\pm\eta_\pi},\ \mathrm{e}^{\pm\tilde{\eta}_\mu}$. See Table 3 for $[G_0;\ g_{1,0},\ g_{2,0}]$.

$g_1(Q)$ and/or $g_1^\dagger(Q)$	$g_2(Q)$ and/or $g_2^\dagger(Q)$	$G(Q)$ and/or $G^\dagger(Q)$
$g_1(Q) = g_{1,0}G(X)$	$g_2(Q) = g_{2,0}\left[\ln\dfrac{Q}{2\tilde{\gamma}_\mu} - \dfrac{G(Q)}{G_0}\right]$	$G(Q) = Q^2 - \dfrac{4}{9}Q^3\mathrm{e}^{-\xi\tilde{\eta}_\mu}$
$g_1^\dagger(Q) = g_{1,0}G^\dagger(Q)$	$g_2^\dagger(Q) = g_{2,0}\left[1 - \dfrac{G^\dagger(Q)}{G_0}\right]$	$G^\dagger(Q) = 2Q^2 - \dfrac{4}{3}Q^3\mathrm{e}^{-\xi\tilde{\eta}_\mu}$

Table 3

Explicit forms of $[G_0;\ g_{1,0},\ g_{2,0}]$, and their numerical values for electron ($\xi = 1$) and positron ($\xi = -1$).

$[G_0;\ g_{1,0},\ g_{2,0}]$	$\xi = 1$ (e^-)	$\xi = -1$ (e^+)
$G_0 = \dfrac{2}{3}\dfrac{1+(2\xi-3)\tilde{\beta}_\mu}{1-\tilde{\beta}_\mu}\,\mathrm{e}^{2\tilde{\eta}_\mu}$	1.163	-0.570
$g_{1,0} = \dfrac{m_\pi}{m_\mu}\tilde{\gamma}_\mu(3-\xi\tilde{\beta}_\mu)$	3.745	4.490
$g_{2,0} = \dfrac{1}{6}\dfrac{m_\pi}{m_\mu}\dfrac{\tilde{\gamma}_\mu}{\tilde{\gamma}_\mu^2-1}(\xi+5\tilde{\beta}_\mu)$	6.780	1.027

Table 4

Numerical values of coefficients appearing in the multiplicity given by Equation (27) for various kinds of secondaries s.

s	$\bar{N}_0$	E_{th}(GeV)	ϵ_c(GeV)	k
γ	8.80	0.28	0.021	1.0
π^+	4.40	0.29	0.021	1.0
π^-	3.80	0.76	0.286	0.5
K^+	0.38	2.50	0.021	1.0
K^-	0.28	15.0	0.286	1.0

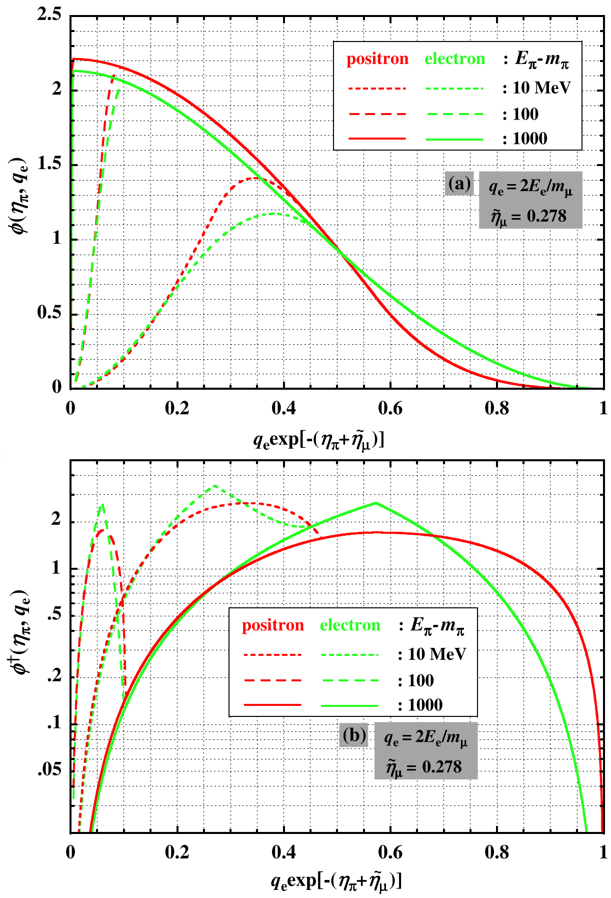

Fig. 1.— Numerical values for (a) $\phi(\eta_\pi, q_e)$ and (b) $\phi^\dagger(\eta_\pi, q_e)$. For $\epsilon_\pi(\equiv E_\pi - m_\pi)$ larger than 1 GeV, both ϕ and $\phi^\dagger$ scales in the form of E_e/E_π, as $q_e \exp(-\eta_\pi) \propto E_e/E_\pi$.

Table 5

Numerical values of the coefficients appearing in the source energy spectrum given by Equations (60) and (61).

source flux	$\beta = 2.6 (\gamma = 2.27)$	$\beta = 2.7 (\gamma = 2.37)$	$\beta = 2.8 (\gamma = 2.47)$
$Q_{0,\mathrm{p}}$ ($\mathrm{m^{-3}s^{-1}GeV^{-1}}$)	6.909×10^{-18}	1.092×10^{-17}	1.928×10^{-17}
$Q_{0,\mathrm{e}}$ ($\mathrm{m^{-3}s^{-1}GeV^{-1}}$)	2.513×10^{-20}	4.236×10^{-20}	7.110×10^{-20}

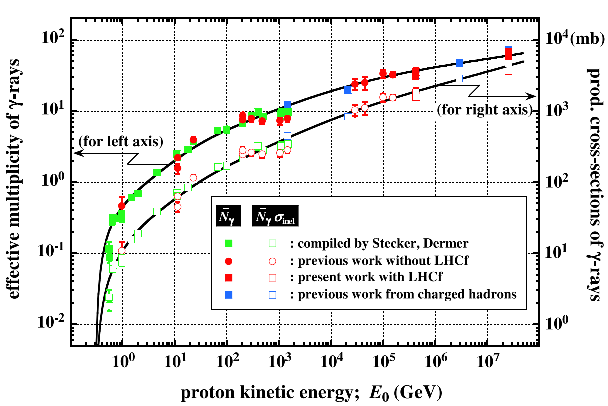

Fig. 2.— Average γ-ray multiplicity, $\bar{N}_\gamma$, for the left axis, and the production cross-section, $\sigma_{\mathrm{inel}}\bar{N}_\gamma$, for the right axis against the proton kinetic energy E_0. See Paper I and the references therein for the data.

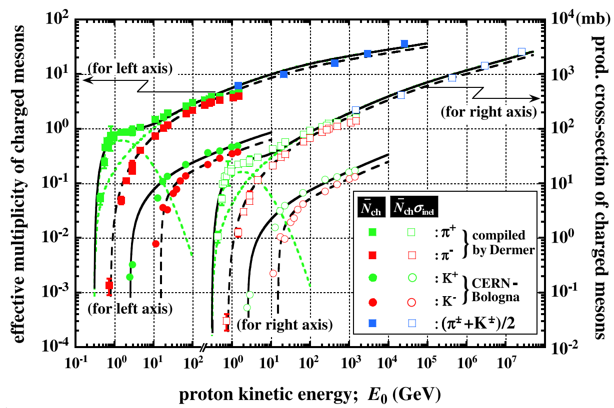

Fig. 3.— Same as Figure 2, but for charged mesons, $\pi^\pm$ and $\mathrm{K}^\pm$. In the case of charged pions, we present separately two contributions from the pionization and isobaric components with both green dotted curves, and superposed ones with heavy solid (π^+, K^+) and heavy dotted (π^-, K^-) ones.

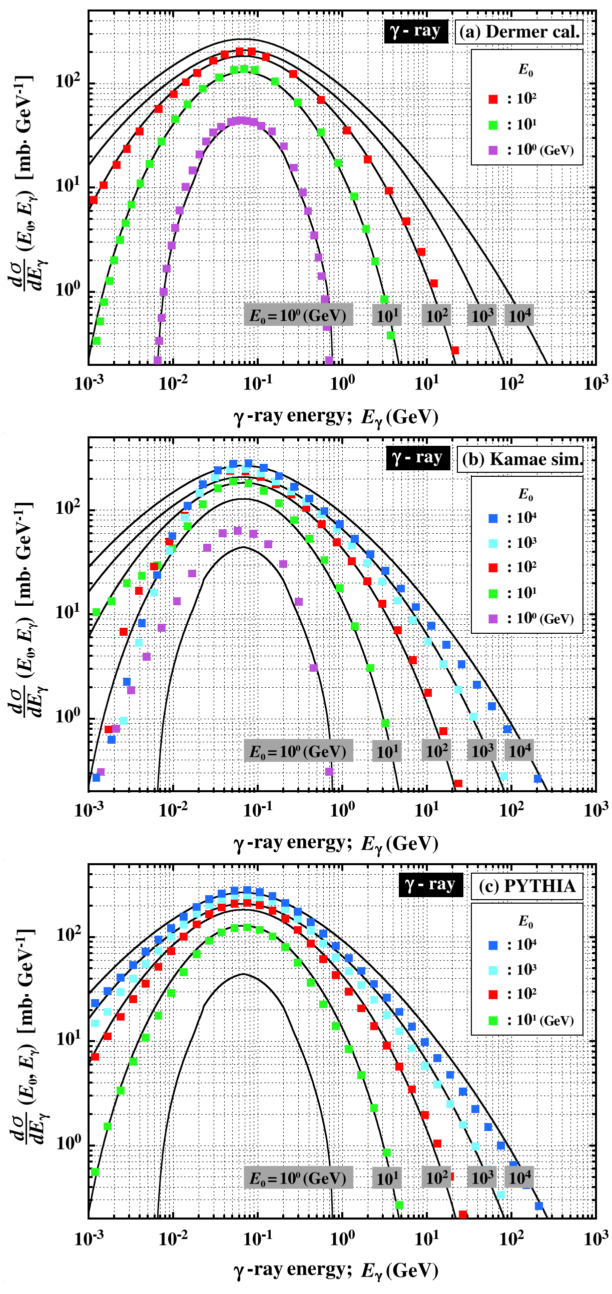

Fig. 4.— Comparison of the present empirical production cross-section of γ-rays (heavy solid curves) with three numerical results, (a) Dermer (1986), (b) Kamae et al. (2006), and PYTHIA-code (Sjostrand et al. 2006), for $E_0 = 10^0, 10^1, 10^2, 10^3, 10^4$ GeV (squared symbols).

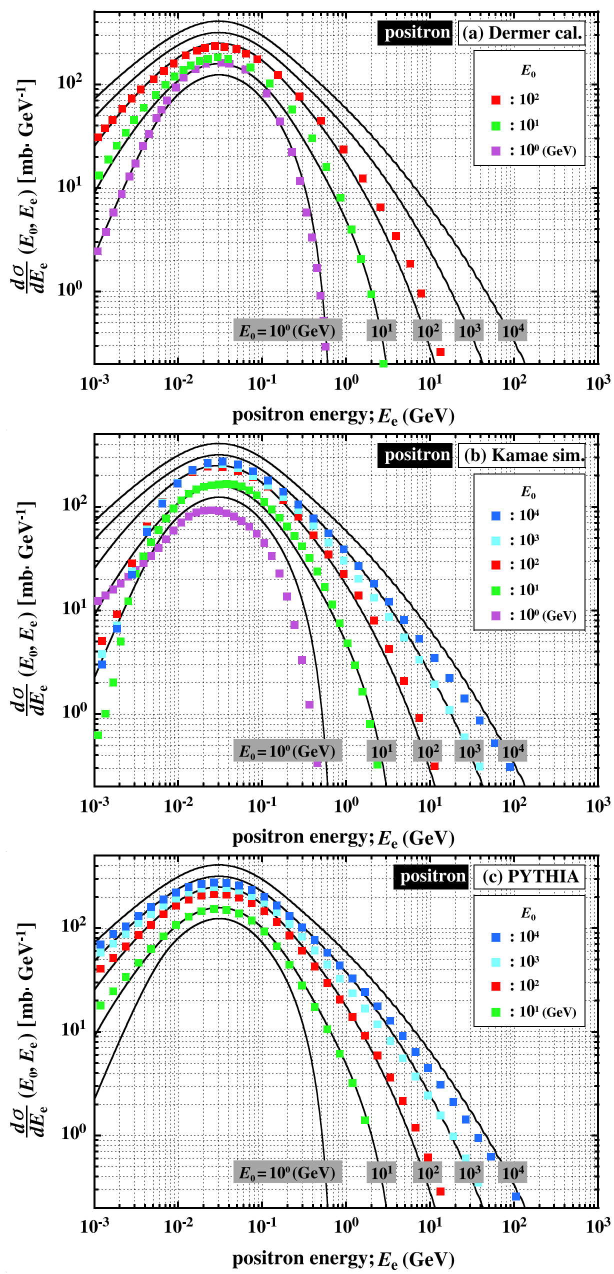

Fig. 5.— Same as Figure 4, but for the production cross-section of positron.

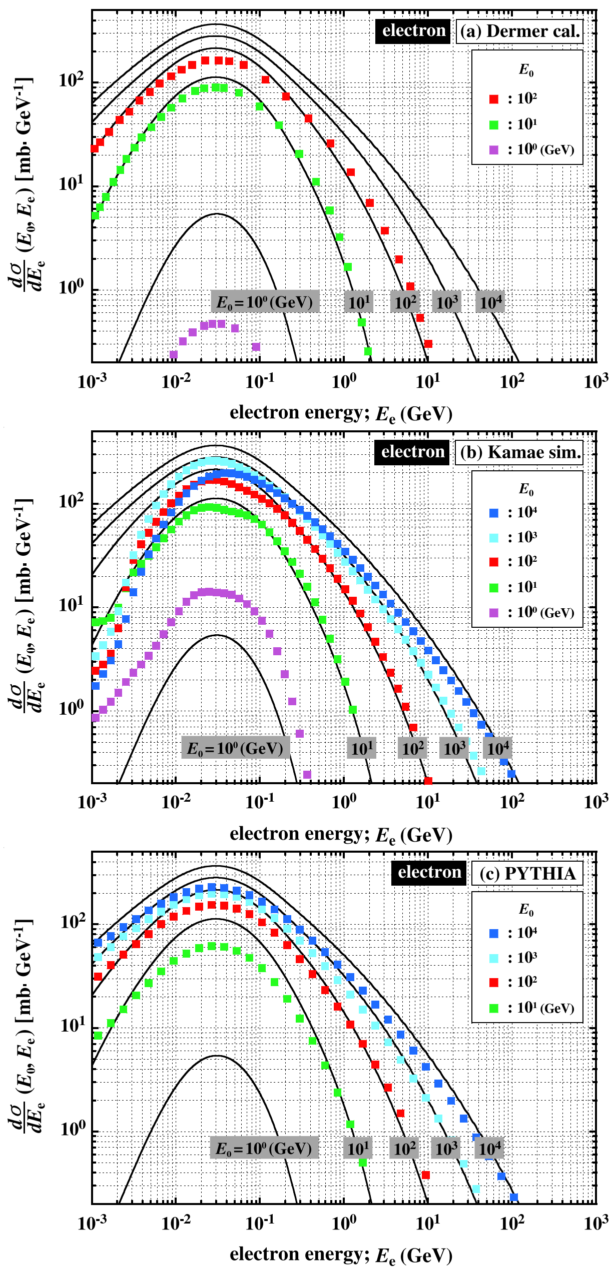

Fig. 6.— Same as Figure 4, but for the production cross-section of electron.

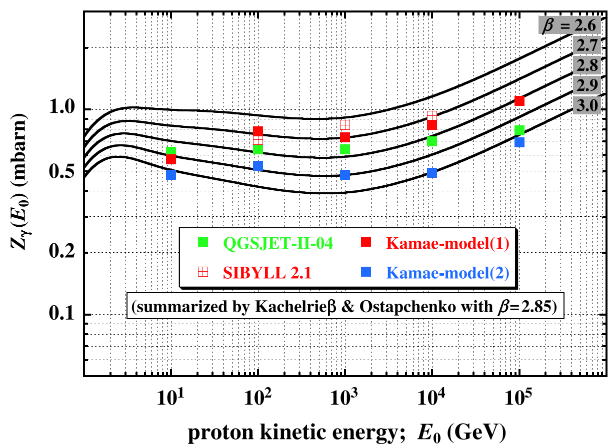

Fig. 7.— Comparison of the numerical vaule of the spectral-weighted moment in γ-ray yield, $Z_\gamma(E_0)$, where our curves (heavy solid ones) present those in the five cases of spectral indices, $\beta = 2.6$, 2.7, 2.8, 2.9, and 3.0, while simulational ones assume $\beta = 2.85$.

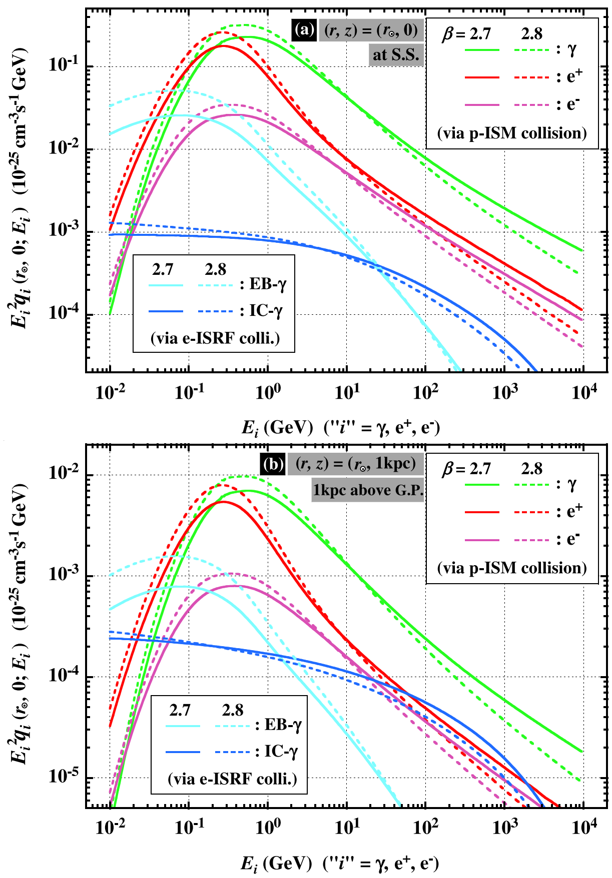

Fig. 8.— Emissivities of γ (green), e^+ (red), and e^- (purple) induced by the collision between CR-proton and ISM, taking account of the nucleus effect (see Section 8 for the explicit corrections), at two observtional sites, (a) SS, and (b) 1 kpc above the galactic plane (GP) with $r_\odot = 8.5\,\text{kpc}$, where we calculate them in the case of $\beta = 2.7$ and 2.8. For the comparison, we present γ's induced by primary electron interactions with the ISM (EB) and ISRF (IC).

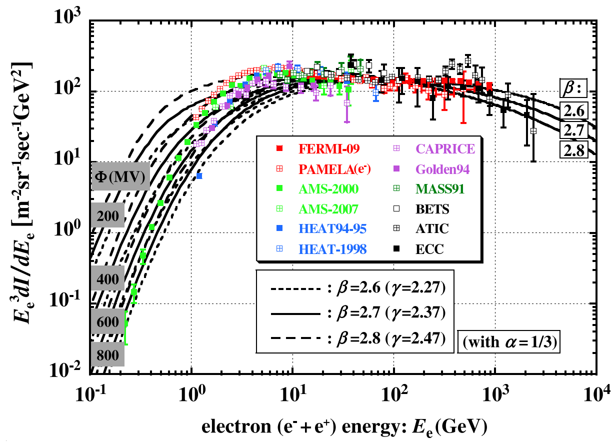

Fig. 9.— All electron spectrum ($e^+ + e^-$) from current data, together wtih the present calculations in the cases of $\beta = 2.6$, 2.7, and 2.8. Numerical curves are all normalized to $E_e = 100\,\text{GeV}$.

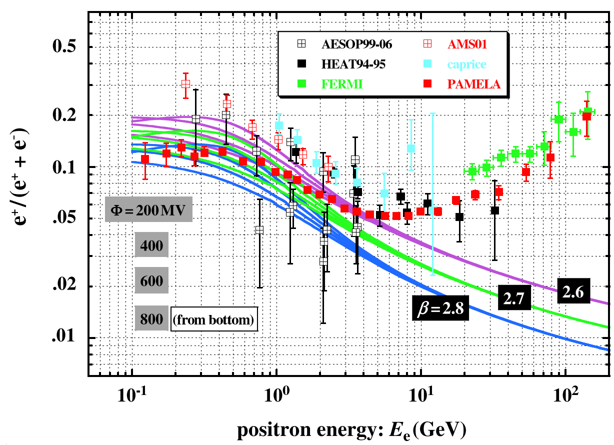

Fig. 10.— Positron fraction currently available, together with our calculations based on the production cross-sections presented in the present work, where we assume three spectral indices, (a) $\beta = 2.6$, (b) $\beta = 2.7$, and (c) $\beta = 2.8$. See Adriani (2009b) and references therein for data.

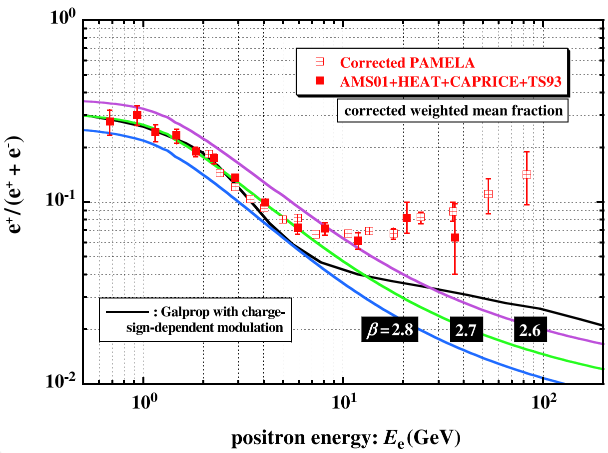

Fig. 11.— Positron fraction after the correction for the charge-sign-dependent solar modulation effect according to the GALPROP code based on the drift model, both for the data and the calculations.

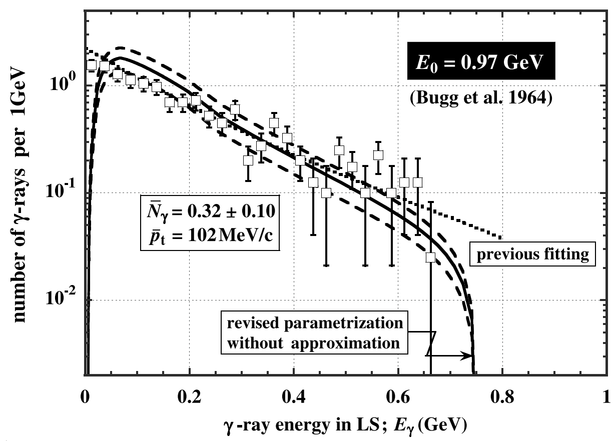

Fig. 13.— Production cross-section of γ's at $E_0 = 0.97$ GeV, where we present empirical ones both from the old one (dotted curve) and the revised one (heavy solid one).

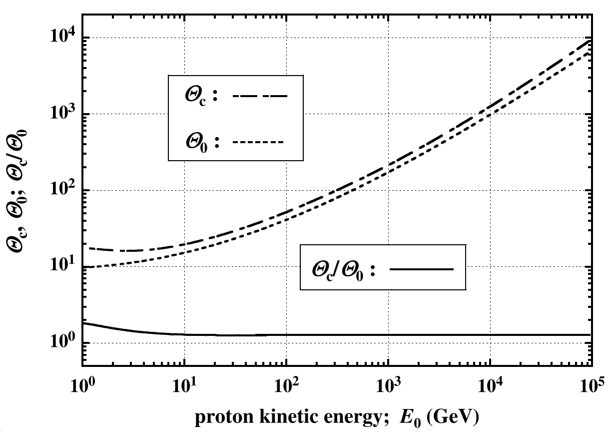

Fig. 12.— Comparison of the previous normalization constant Θ_0 with the present one Θ_0, with use of x_γ in place of x.

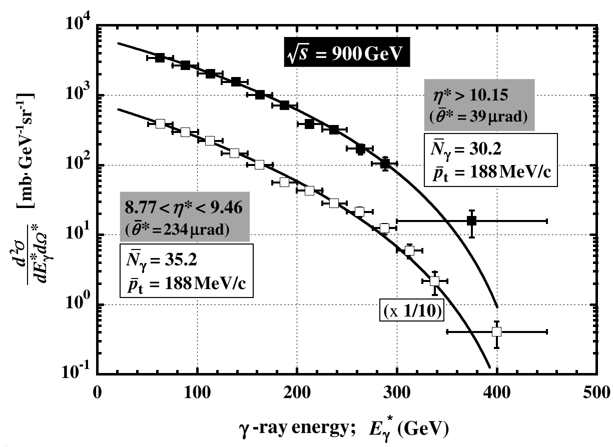

Fig. 14.— Comparison with our parameterization for the cross-section with those observed by the most recent LHCf expriment at $\sqrt{s} =$ 900 GeV, correspondint to $E_0 \approx 400$ TeV.